IAC-18-F1.2.3

Capturing and deorbiting Envisat with an Airbus Spacetug. Results from the ESA e.deorbit Consolidation Phase study.

Stéphane Estable[a]*, Clément Pruvost[b], Eugénio Ferreira[b], Jürgen Telaar[a], Michael Fruhnert[a], Christian Imhof[b], Tomasz Rybus[c], Gregory Peckover[d], Robert Lucas[d], Rohaan Ahmed[d], Tomohisa Oki[d], Marcin Wygachiewicz[e], Pawel Kicman[f], Artur Lukasik[f], Nuno Santos[g], Tiago Milhano[g], Pedro Arroz[g], Robin Biesbroek[h], Andrew Wolahan[h]

[a] *Airbus Defence and Space GmbH, Airbus Allee 1 28199 Bremen,* stephane.estable@airbus.com, juergen.telaar@airbus.com, michael.fruhnert.external@airbus.com, christian.imhof@airbus.com
[b] *Airbus Defence and Space SAS, 31 rue des Cosmonautes, 31402 Toulouse, France*, clement.pruvost2@airbus.com, eugenio.ferreira@airbus.com
[c] *Space Research Centre (CBK PAN) Bartycka 18A, 00-716 Warsaw, Poland,* trybus@cbk.waw.pl
[d] *MDA Inc., 9445 Airport Road, Brampton, Ontario Canada, L6S 4J3,* Gregory.Peckover@mdacorporation.com, Robert.Lucas@mdacorporation.com, Rohaan.Ahmed@mdacorporation.com, Tomohisa.oki@mdacorporation.com
[e] *SENER Sp. z o. o., Aleje Jerozolimskie 202, 02-486, Warsaw,* marcin.wygachiewicz@sener.pl
[f] *GMV Innovating Solutions Sp. z o.o., Hrubieszowska 2, 01-209 Warsaw, Poland,* pkicman@gmv.com, alukasik@gmv.com
[g] *GMV Skysoft, Av. D. João II, nº 43, Torre Fernão de Magalhães 7º, 1998-025 Lisboa, Portugal,* nuno.santos@gmv.com, tmilhano@gmv.com, parroz@gmv.es
[h] *ESTEC, Keplerlaan 1, 2201 AZ Noordwijk, The Netherlands,* robin.biesbroek@esa.int, andrew.wolahan@esa.int
* *Corresponding Author*

Abstract

Airbus has been developing a mission and chaser concept for capturing and deorbiting the defunct Envisat satellite with different partners in the frame of ESA studies (e.Deorbit Phases A and B1). In the last e.Deorbit study called 'Consolidation Phase' which aims at implementing findings from the intermediate SRR, Airbus along with their partners CBK, MDA, SENER and GMV was pursuing the mission and chaser definition, but then based on the Airbus Spacetug vehicle for GEO servicing.

The assumption for this analysis was a Spacetug vehicle adapted for the specific e.Deorbit mission rather than generic electrical Spacetug for orbit transfer or GEO servicing missions. As the same Eurostar Neo bus platform would be used in both cases, the potential for the reuse of the e.Deorbit Spacetug solution for further servicing missions would be therefore very high.

Starting from mission analyses, an e.Deorbit Spacetug baseline configuration was defined, bringing various options depending on the mission scenarios. As with the Airbus Spacetug vehicle, this e.Deorbit Spacetug vehicle aims at being launched with a medium or heavy launcher. The first considered scenario is the one inherited from e.Deorbit Phase B1 study, i.e. based on motion synchronization with Envisat now preceded by a contactless detumbling maneuver, capture via robotic arm and fixation and stabilization using clamping mechanism, before deorbiting with controlled re-entry. The Airbus Spacetug preliminary design is based on the Eurostar Neo platform from Airbus and made of a 2.5kW electrical power system, a chemical propulsion system with associated bi-propellant tanks, a set of sensors dedicated to AOCS/GNC, a robotic arm system, gripper and clamping mechanism for servicing and an On-Board Computer and avionics bus reused from Eurostar Neo.

The preliminary assessment of the synergies between the e.Deorbit and GEO Spacetug systems already shows very good opportunities for a mutual fertilization of both systems. A great opportunity pointing out here is the high flexibility of the Spacetug platform to adapt to different mission configurations.

Keywords: Envisat, capture, removal, robotic, space tug, uncooperative target

1. Introduction

According to ESA [1], today's space debris environment poses a hazard to the safety of operational spacecraft in space and of people and property on Earth. As of November 2015, more than 5100 launches had placed some 7200 satellites into orbit, of which about 4100 remained in space. Only a small fraction - about 1100 - are still operational today. These are accompanied by almost 2000 spent orbital rocket bodies and a large number of fragmentation debris, caused by the break-up of more than 200 objects, as well as mission related objects. This large amount of space hardware has a total mass of more than 8000 tonnes.

The Inter-Agency Space Debris Coordination Committee (IADC) [2] defined two protected orbital regions, an idea which, in 2007, was endorsed by the United Nations General Assembly [3]. The first is the Low Earth Orbit (LEO) protected region which extends from the lowest maintainable orbital altitude up to a height of 2,000 km above the surface of the Earth. The second is the geosynchronous orbit (GEO) protected region, which includes the volume of space bounded in altitude by +/- 200 km of the geosynchronous altitude (35,786 km) and in inclination by +/- 15 degrees.

More than 23.000 space objects in total (around 17.000 of which published) are regularly tracked by the US Space Surveillance Network and maintained in its catalogue, which covers objects larger than approximately 5 to 10 cm in LEO and larger than 30cm to 1m at geostationary altitudes (GEO). LEO is the most congested region in near-Earth space, containing approximately 75% of all catalogued objects. At typical collision speeds of 10 km/s in low orbits, impacts by debris larger than about 10 cm are expected to cause catastrophic break-ups i.e. the complete destruction of the spacecraft with a resulting fragmentation event and production of many pieces of smaller debris. For objects too small to catalogue, the population levels are even greater. For instance, the number of debris between 1 and 10 cm is assessed to be several hundred thousand, and the number between 1 mm and 1 cm is assessed to be in excess of 100 million [4].

Since 2005, some IADC members have been assessing, under a variety of space debris mitigation scenarios [5], the stability of the LEO space object population and the need to use active debris removal (ADR) to stabilize the future LEO environment. ASI, ESA, ISRO, JAXA, NASA, and UKSA (the six IADC members that have been principal participants in the study on Stability of the Future LEO Environment) employed their own environment evolution models under a common set of initial conditions and assumptions, reaching very similar results. The study confirmed that the current LEO object population will grow even in a scenario with full compliance with existing national and international space debris mitigation guidelines. To stabilize the LEO environment, first of all, mitigation measures need to be applied to the required level, but also additional measures, in particular the active removal of the more massive non-functional spacecraft and launch vehicle stages, should be considered and implemented in a cost-effective manner [6].

During the e.deorbit Active Debris Removal (ADR) studies carried out by ESA, ENVISAT was used as the debris Target. This selection was based on several criteria. ENVISAT is one of the few ESA-owned space debris in the densely populated near-polar region in the 600-800 km altitude band. It is also the debris object with the highest collision risk of all ESA objects. Its heavy mass (8 tonnes) and large size makes it representative of the many heavy space debris objects such as the many Zenit 2 SL-16 stages. By targeting ENVISAT, the e.deorbit mission will remove the largest mass that ESA owns in orbit.

Another reason for studying ENVISAT removal is the complex capture. This is caused by the tumbling motion of ENVISAT, that forces the e.deorbit Chaser to synchronize its attitude with that of the debris in case of a capture with a robot arm. Furthermore, the solar panel is locked in an unfavorable position, partially blocking the access to one of the strongest and stiffest external points on ENVISAT: its launcher adapter ring (LAR).

The combination of its large mass, complicated capture access, and high collision risk with debris in its current orbit, makes ENVISAT the perfect though ambitious Target for the first ever ADR mission, providing an opportunity for European industry to show case their technological capability to a global audience.

Airbus was leading different consortia since 2014 to work on the ESA e.Deorbit studies Phase A [22], Phase B1 [23] and currently in 2018 the Consolidation Phase. The aim of the Consolidation Phase implemented with Space Research Centre CBK PAN, GMVIS SKYSOFT S.A., GMV Innovating Solutions Sp. z o.o., MDA and SENER Sp. z o.o. is to further work on specific topics selected by ESA after the intermediate SRR like mission definition and communication blockages, simulations (GNC, coupled control, visual servoing and compliant control) and the spacecraft definition including the robotic subsystem. In this study phase the spacecraft is based on the Airbus Space Tug for Geo-Servicing with adaptations to the specificities of the e.Deorbit mission. This paper will present the main results obtained during the Consolidation Phase in these different domains and for the space tug definition dedicated to the capture and removal of space debris.

2. e.Deorbit mission definition

2.1 Mission Description

Fig. 1 provides an overview of the mission phases. The Chaser enters Safe Mode following launch into the Target's 760 km circular injection orbit. Subsequent to the LEOP and initial Commissioning, the Chaser commences the orbit injection correction and phasing. During this phase the Chaser is alone and relies on absolute navigation. The Chaser's GPS and TLE data for the target are used to calculate the required manoeuvres. The phasing ends in Far Formation Flight based on absolute navigation and relative orbital elements (ROE) control. In this mode the Chaser is in a passively safe relative orbit with e/i-separation at a safe distance behind the target. Once this is reached, the far range camera is switched on for the target acquisition. In this mode the Chaser's attitude is commanded to

target pointing. After confirmation from ground that the target is correctly identified, the Chaser is transitioned to a relative navigation based on far range camera LOS measurements. This transition involves a period of sensor calibration where there is an overlap between absolute and relative. At a distance of approximately 8km and a pointing towards Envisat, the relative navigation based on the far range camera (CAM-N) will be initiated. After far-range relative navigation, it must be ensured that the navigation filter has converged and that the correct target has been selected. The decision on the continuation will be made on ground and is based on the comparison of absolute and relative navigation. The Chaser then commences the spiral approach to the Safe Hold Point. The delta-V necessary for the spiral approach is executed by the RCS thrusters.

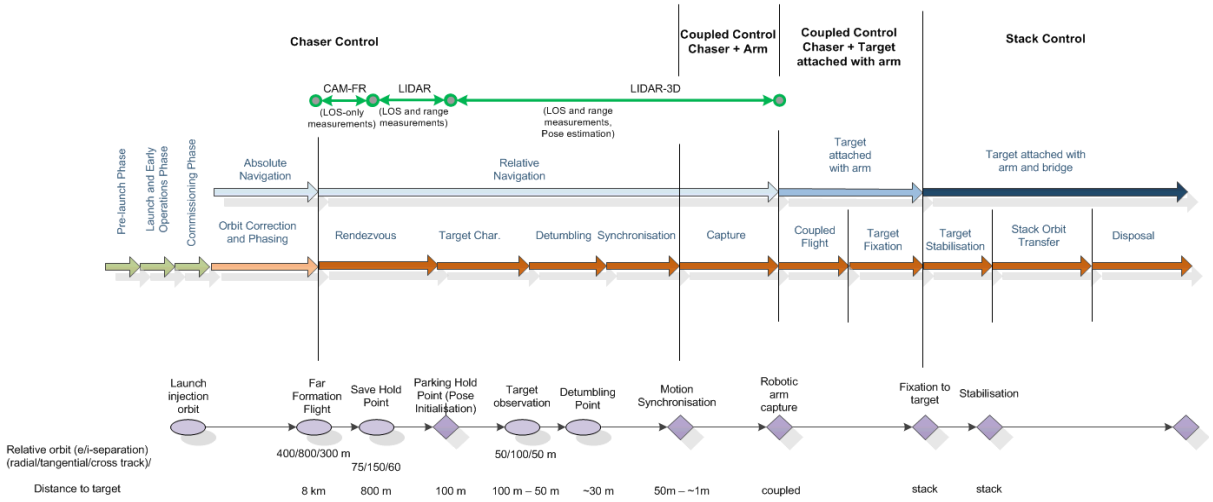

Fig. 1. Mission phase overview

At the Safe Hold Point, a passively safe relative orbit with e/i-separation, the LIDAR is switched on. The LIDAR provides LOS and range measurements. Once the LIDAR navigation filter has converged, it becomes the primary navigation sensor. The next spiral approach ends at the Parking Hold Point at approximately 100 m distance on the v-bar behind the target, leaving the passively safe e/i separated relative orbit and entering forced motion position control.

At the Parking Hold Point the LIDAR is switched to the LIDAR 3D mode and performs a pose estimation. Then the far range camera takes the first images of the tumbling Envisat.

The inspection flight then occurs following a command from ground. The inspection flight is again on an e/i separated relative orbit to ensure safety. Once it is completed, the Chaser retreats to the Parking Hold Point where it waits until the ground is satisfied with the characterisation of Envisat. It may be necessary to upload new software to the Chaser if Envisat behaviour is not as envisaged. The timeframe for this upload is expected to be in the order of days. It is not foreseen to develop completely new software; rather, what could be necessary is an update of the model of the target in case of unforeseen damages.

The target tumbling characterisation is performed first to decide how to fly around the target, to ensure the most suitable images and views are attained. This is carried out by acquiring LIDAR acquisition at the Safe Hold Point (with some images). The Chaser then waits for data download (investigation of sensor data on ground in parallel) and battery charging. The Chaser then moves to the Parking Hold Point and then performs the inspection fly-around. The chaser then retreats again to the safe hold point and the inspection images are downloaded. Battery charging is also performed and the on-board model is updated. The arm is unfolded and the Chaser moves again to the Parking Hold Point.

Once the Chaser is commanded from the ground to do so, it enters the Synchronised Flight Phase, and then the Target Capture Phase. The synchronisation and capture, are performed autonomously on-board the Chaser with monitoring from the ground, with the ground commanding the commencement of the Capture Phase. During these phases a CAM (Collision Avoidance Maneuver) can be triggered, either by ground or by the on-board safety monitoring function.

The arm then grasps the Target and the Chaser confirms this on-board and immediately rigidizes the robotic arm. This means that the joint stiffness is progressively increased for stopping the relative motion. Once the relative motion is zero the brakes are set. The ground then confirms that it agrees that capture and rigidisation have been executed. Next is the short coupled flight phase while waiting for the ground “go” decision. After the positive decision, the Target Fixation

Phase starts when the arm breaks are unlocked and the SpaceTug is moved for clamping operations.

Clamp fixes to the Target, with monitoring from ground via a monitoring camera and sensor data (pressure and force sensors) to confirm the clamping. Then, rigidizes and is trimmed for CoG alignment. After the CoG ground analysis the clamp is rigidized. Robotic arm releases the Target's LAR and performs the solar array boom grapple to secure solar array during further operations. Having the stack securely connected, the Target Stabilisation Phase is performed. The angular motion of the coupled system is then measured to calculate the de-tumbling sequence and stabilisation is performed. Following de-tumbling, the coupled system is slewed to a sun-pointing attitude in order to re-charge the batteries.

After confirmation from ground, the stack is re-oriented for the Stack Transfer Phase (2 burns) and the Disposal Phase, which includes target passivation to ensure safe re-entry (1 burn).

2.2 Contactless detumbling

To detumble Envisat the plume impingement contactless detumbling method is proposed. The method consists of using the gas jet exhaust from a thruster mounted on the chaser to influence the target. This method can be used for de-orbiting (imparting a delta-V) or for detumbling (momentum transfers). The attitude and angular rate of the target are controlled by pointing the thruster to different regions of the target's surface. The pointing of the thruster is performed by controlling the attitude of the chaser.

In order to test the feasibility and effectiveness of the proposed method, a simulator used in a previous activity – COBRA – was repurposed for this activity. The COBRA simulator is presented in [7] as it also concerns the detumbling of Envisat via plume impingement.

In the test scenario, the chaser performs station-keeping, 30 m from Envisat, perpendicular to the initial angular momentum of the target. The spin axis in body frame is randomly aligned, angle between YsZs plane and spin axis is limited to 30° (close to flat spin),the initial spin rate has a 2.5 degrees per second mean plus 0.1 deg/s standard deviation on the three components and the scenario has a duration of 8 hours. The results were obtained by performing a 50 runs Monte Carlo test.

The results can be seen in Fig. 2, which represents the norm of the target angular rate versus time and in Fig. 3 which represents the residual angular rate magnitude versus its angle with respect to the axis of less inertia.

The results show that it is feasible to reduce the target's angular rate using the plume impingement method. After 8 hours of detumbling, the target's angular rate was reduced from 2.5 to an average 0.4 deg/s, with a dispersion of 0.3 deg/s (1-sigma). Furthermore, the average direction of the angular rate is aligned with the axis of less inertia, with a 1-sigma dispersion of 30 degrees, and the largest residual rates are observed aligned with the axis of less inertia. This is unsurprising since, due to the geometry of the target, the x-axis is the most difficult to de-spin. Although the presented results correspond to an 8 hour scenario, the results are not much different from the ones obtained at the 4 hours mark. This shows that, as the target spins slower, the effectiveness of the method in de-spinning the target further decreases.

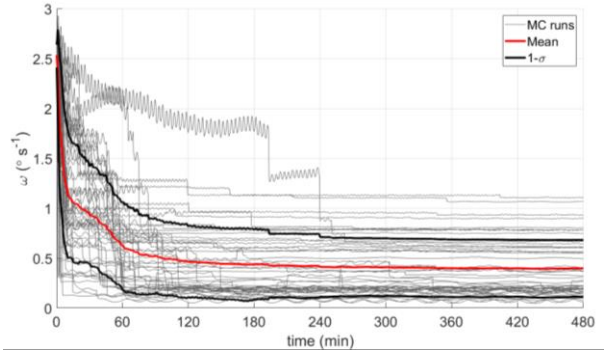

Fig. 2. Target angular rate versus time

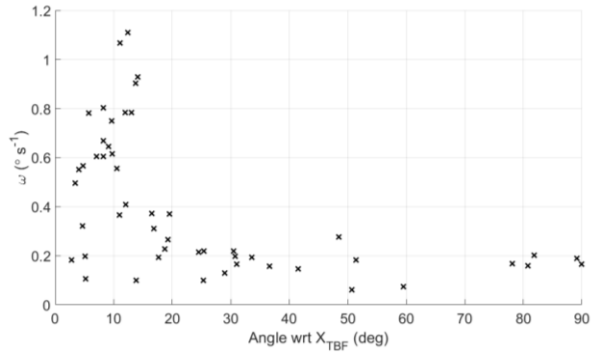

Fig. 3. Target residual angular rate versus direction

3. Communication blockage analysis

3.1 Geometrical blockage analysis

This section presents the analysis the communication blockages produces after capture. The Chaser has two Antennas to communicate with the Ground Stations, Antenna 1 and 2. After capture of Envisat, some elements of Envisat block at some points the connection, in particular the solar panel and the ASAR antenna.

Example Space Tug antenna configuration is presented in Fig. 4. The analysis has taken into account the synchronisation and capture trajectory from GNC simulations for the rotational speed of the Target of 0.5°/s. For the timeframe of 28 days, for each communication session the same trajectory was realised for as long as the communication session lasted –

sometimes it did not realise the whole trajectory and sometimes it remained frozen at the capture point after the whole trajectory was finished. The Target attitude was changing continuously, so for each communication session, the initial attitude of the Target w.r.t. Earth was different. The simulated trajectory was defined w.r.t Target so it was also changing w.r.t. Earth. For each point on the trajectory (3911 points in the complete trajectory, with 1/3 s timestep) the frequency of the blockages has been calculated and an example result is presented in Fig. 5 and results for different configurations and antenna booms is presented in Fig. 6.

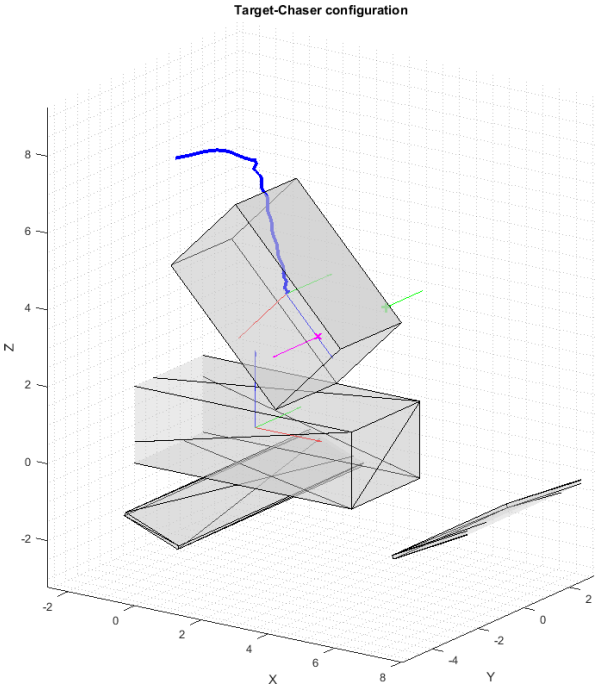

Fig. 4. Symmetrical front antenna configuration visualisation

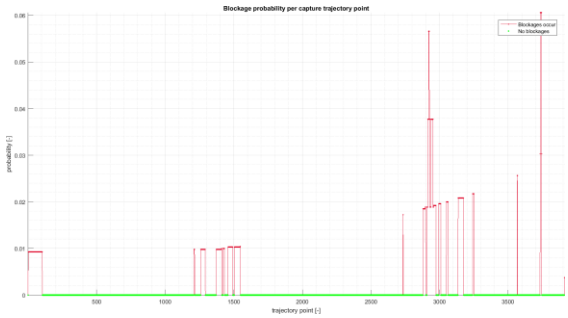

Fig. 5. Blockage probability per capture trajectory point plot for example configuration

	Boom lengths [m]	Blockage windows mean [s]	Blockage maximum [s]	Number of blockages [-]		Boom lengths [m]	Blockage windows mean [s]	Blockage maximum [s]	Number of blockages [-]
Conf 1	0	10.27	66.67	21	Conf 3	0	19.29	95.33	15
	0.5	20.38	55.00	16		0.5	18.91	95.33	11
	1	17.33	43.67	8		1	28.00	95.67	4
	1.5	17.78	23.00	3		1.5	44.67	83.67	2
	2	**0.00**	**0.00**	**0**		2	34.50	64.00	2
Conf 2	0	47.45	123.33	25	Conf 4	0	25.35	67.33	20
	0.5	40.72	112.33	23		0.5	20.22	51.67	15
	1	42.46	100.67	16		1	14.96	36.33	8
	1.5	41.00	88.33	13		1.5	11.25	12.33	4
	2	38.77	74.67	10		**2**	**0.00**	**0.00**	**0**

Fig. 6. Blockage analysis results summary table

In conclusion, only the 2m booms for the antennas are able to ensure the complete mitigation of the blockages during the critical capture phase of the mission.

3.2 Full wave RF analysis

In order to verify the purely geometrical blocking analysis a full wave RF analysis for identified critical points on the trajectory is implemented. Therefore a detailed 3D model of both the chaser as well as the target satellite is created and is analysed using the Multilevel Fast Multipole Method (MLFMM) implemented in the commercial RF simulation tool CST Studio Suite®. This described full wave analysis approach is essential in order to be able to also take into account the generated interferences due to reflection and diffraction of the antenna radiations from the satellites. Additionally the possible interference between the two antennas which are operated at the same time can be addressed in these simulations.

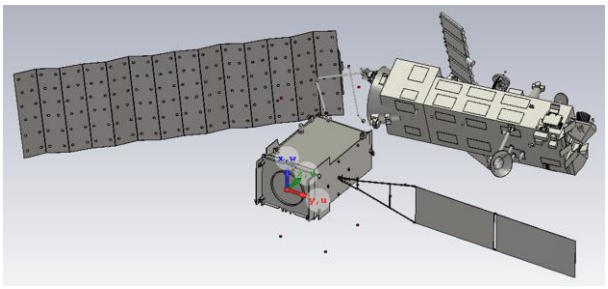

Fig. 7. Geometrical Simulation model for the capture point

The capture point is one of the critical situations which are analysed with the full wave approach. In Fig. 7 the geometrical simulation model can be seen. The total installed pattern being the combination of the

two antennas on the chaser satellite is given in Fig. 8. As can be seen in the plot, besides smaller areas where the gain is influenced by interferences there are no major regions with small gain values visible in the plot. The minimum installed antenna gain is -7.2 dBi in this scenario which is a value that still allows the establishing of the downlink according to the link budget presented in [8], where a minimum antenna gain of -9.9 has been calculated. This leaves a margin of about 2.7 dB for this case so that a complete coverage as indicated by the geometrical blocking analysis can be confirmed in this case.

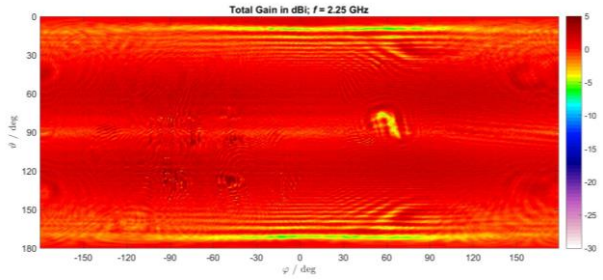

Fig. 8. Simulated total antenna gain for the capture point configuration

4. Simulations

4.1 GNC Simulations

The current section describes control design approach and summarises simulation results for the mission phases: rendezvous and target motion synchronisation.

i. Control synthesis

The control synthesis methodology adopted is H∞ Mixed Sensitivity Design [9]. Its synthesis process aims at shaping the sensitivity functions in order to achieve the closed-loop system performance and robustness requirements. Moreover, the sensitivity function shaping is achieved with frequency varying weights (of MIMO nature). The weight selection as well as the robust stability and performance analysis follows the process in [10,16].

ii. Linear modelling approach

The $\mathbf{H}_{\infty}$ synthesis method adopted [14,15] requires an LFT representation of the linearized flexible spacecraft model so that the plant model can consider parametric variations. An accurate and straightforward modelling technique of a multi-body system is the Two-Input Two-Output Port (TITOP) [11]. Fig. 9 shows the chaser spacecraft instantiation. The hub TITOP starts from its rigid dynamics, with uncertainty on mass and inertia parameters, and is expanded to connect to two child elements: slosh modes, and solar panel flexible modes.

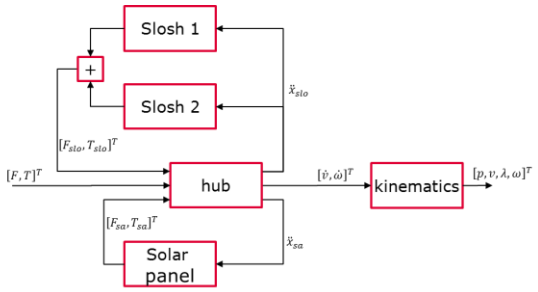

Fig. 9. Chaser model based on TITOP models

iii. Time-domain simulation architecture

Fig. 10 10 schematises the model-in-the-loop simulation architecture for validation of the GNC algorithms during rendezvous and target motion synchronisation phases. Robot arm is not active, relative navigation chain replaced by performance model. The control function issues force and torque commands, converted into thruster commands by the thruster management function.

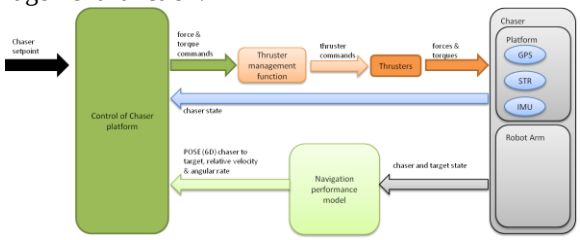

Fig. 10. Chaser model based on TITOP models

iv. Time-domain simulation results

The rendezvous (Fig. 11) comprises all mission phases from so-called Rendezvous Entry Gate at 8km from Envisat, up to Parking Hold Point (PHP) at 100m in V-Bar.

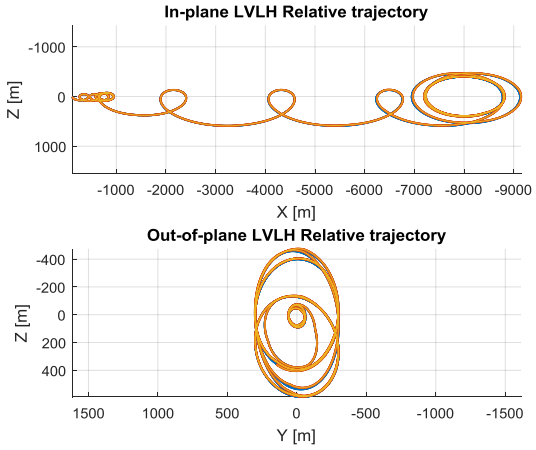

Fig. 11. Trajectory projections for rendezvous phase (blue: reference, gold: real).

As can be seen, it relies extensively on relative safe orbits. Synchronisation (Fig. 12) starts at PHP and,

through a series of forced motion manoeuvres utilizing the Envisat angular momentum direction, finishes at Capture Point. The chaser platform then maintains this point during robot arm operation. The guidance law definition is a further development of that in [12].

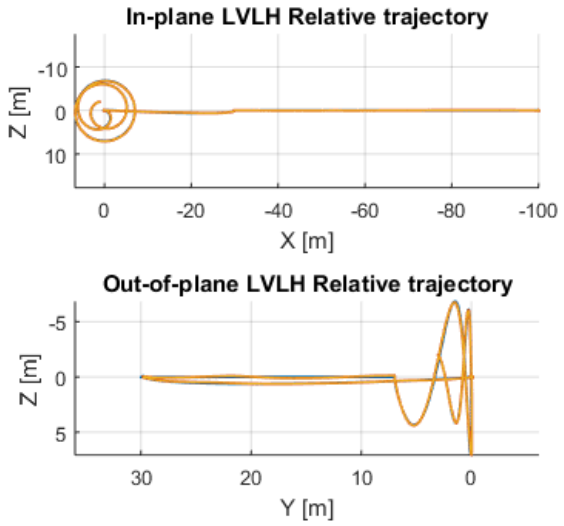

Fig. 12. Trajectory projections for synchronisation phase (blue: reference, gold: real).

A Monte Carlo test campaign was carried out ensuring 95% confidence interval on analysed metrics [13]. Performance requirements were met as specified per control synthesis specification.

4.2 Coupled control design / simulation

The chaser has to perform station keeping at the Capture Point during the grasping operations performed by the robot arm. The aim of the robot arm control is to minimize the error between the current end-effector pose and the desired pose at the grasping point, or otherwise, to follow a reference trajectory. For this scenario, the grasping point is located at the Target's launch adapter ring.

The coupled control structure separates the robotic arm control from the GNC control of the Chaser. The GNC operates relative to the Target in order to control the attitude of the Chaser with a frequency of 1 Hz. The robot controller has a higher bandwidth and its sampling time is 1 ms (1 kHz frequency).

The coupled control simplifies the overall control design. However, both controllers still exchange information and are therefore achieving an acceptable performance. For example, the feed forward term from the robot control to the Chaser GNC provides the forces and torques generated in the arm base by the robot. The guidance estimates the forces and torques required for compensating the centrifugal forces due to the tracking of the desired position and attitude relative to the tumbling target. The Chaser provides the relative pose (position and orientation) between Chaser and Target to the robot controller, and the robot controller exchanges data with the Chaser by means of forces and torques computed at the base of the robot. More details about the coupled control of chaser and robot arm can be found in [17]. The feedback term compensates for uncertainties and disturbances.

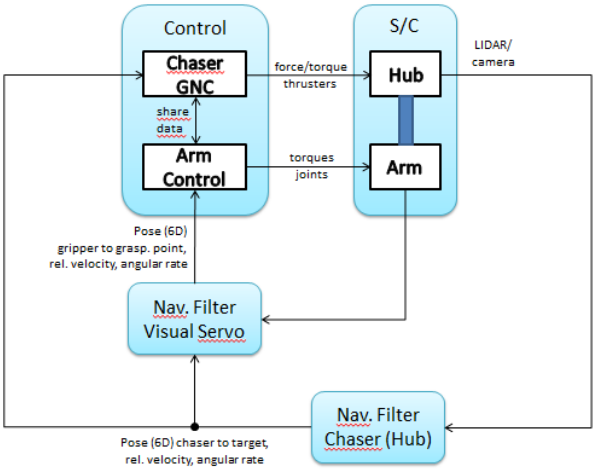

Fig. 13. Coupled Control Principal

In principal, the Chaser is a free-floating platform and every movement of the chaser affects the motion of the robotic arm and vice versa. This interaction has a significant impact on the accuracy and precision of the robotic end-effector.

The simulation is designed to capture the impact of a variety of disturbances. It has been assumed that the movement of the robotic arm is quick relative to the orbital motion. Therefore, most of the external disturbances like third body perturbations, radiation pressure, etc. were neglected, and the setup focused on the internal disturbances like fuel sloshing of the tanks and flexible modes of the Chaser's solar array. Simplified models for fuel sloshing and flexible modes were taken into account to make an informed robust control design, which was not overly conservative.

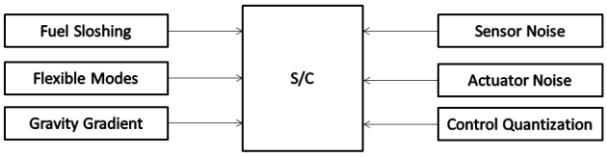

Fig. 14. Modelled Sources of Disturbances

The model of the gravitational field of the Earth included spherical harmonics up to third order and was expected to have little impact on the control performance.

A more relevant source of error is the noise of the sensors used to determine the relative pose (position and orientation) of Chaser and Target and Gripper and

Grappling Point. For example, the primary relative navigation sensor for the coupled control phase is a LIDAR, which allows full relative pose estimation. The accuracy of the visual based navigation can vary on the current position and orientation of the bodies, changes with distance, and introduces noticeable latencies into the feedback loop.

The major source of disturbances, however, is based on the movement of the chaser. If it moves quickly, then the fuel in the tanks starts to slosh more and the flexible structure of the solar array starts to shake the spacecraft. Additionally, the control of the thrusters is limited in bandwidth and, in reality, is quantised. Those effects are considered in the nonlinear simulation, which will test and validate the control that was designed with a simpler structure.

A configuration assembled of Two-input Two-output Port (TITOP) models [18] is used to quickly linearize and analyse the system response, which will then be confirmed with a Monto Carlo campaign using the full nonlinear model that was created in MATLAB/Simulink R2017a and makes use of the Simscape extension to model the multi-body dynamics.

Incorporating the TITOP model has the advantage that for example the fuel slosh and the flexible mode can be easily modelled as structured disturbance in a linear setup. Hence, it will be straightforward to apply MATLAB/Simulink's design tools to generate a robust and performant control design, which can then be tested and validated against the nonlinear simulation.

4.3 Visual Servoing simulations

During the capture phase the vision system, consisting of laser pattern projectors, monochrome cameras, and optical filters, mounted on the LAR gripper provide 6 DOF POSE estimates of the Envisat's LAR with respect to the gripper by means of 3D model matching.

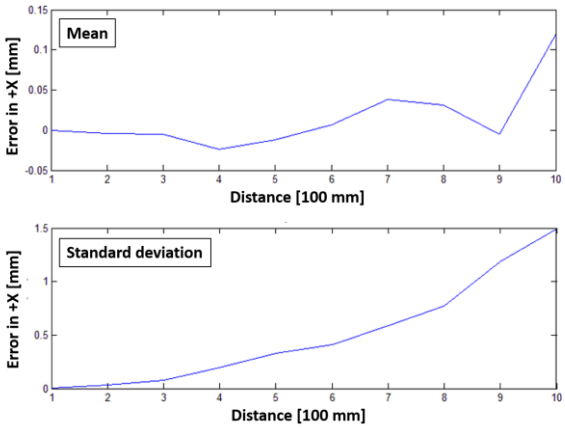

Fig. 15. Mean and standard deviation of POSE error in +X

This POSE information, via visual servoing, is used to guide the robotic arm to the capture position. Mean and standard deviation for the POSE estimate error were determined as a function of distance between the LAR and the gripper during Phase B1 (Fig. 15 and 16). Using this data, an error model was established for the Consolidation Phase and used in dynamic simulations for the purpose of assessing the visual servo control system.

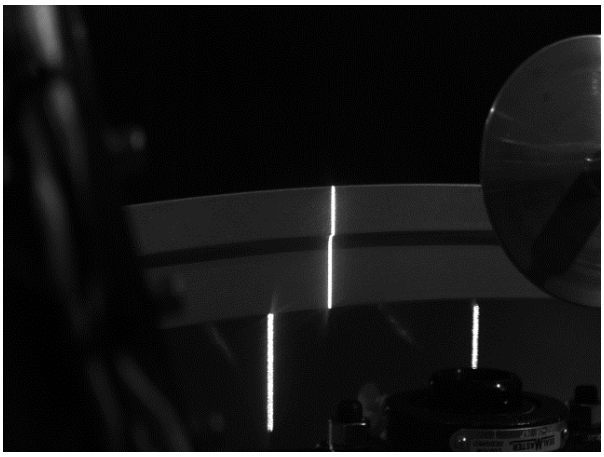

Fig. 16. LAR with the laser line produced by the vision system proposed during Phase B1

Fig. 17 shows a simulation flowchart for the 6 DOF POSE estimation during a dynamics simulation loop. Initially a true POSE is obtained from true system variables (e.g. position and orientation of chaser and target, joint angles of the robotic arm). POSE estimates are computed with the error model, which is then sent to the visual servoing algorithm where the POSE estimates are used to determine the arm tip control commands based on a conventional PD feedback scheme. The arm tip commands are then tracked by the robotic controller. Dynamic simulations were performed to assess the performance of the visual servo control system. In the example below, the target (Envisat) has initial angular velocity of 2.5 deg/s in +Z in the target body frame and there is no residual linear and angular velocities between the target and chaser at time = 0 [sec]. During the simulation, the SpaceTug GNC was turned off, allowing the free-floating motion of the chaser body. The chaser's robotic arm was able to achieve and maintain alignment to within the LAR Gripper capture envelope guided by the visual servo algorithm (Fig. 18).

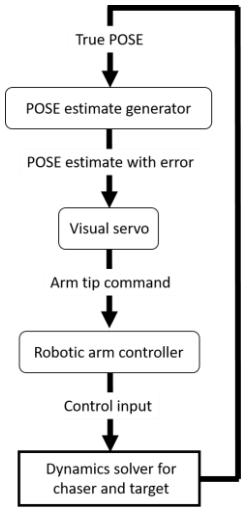

Fig. 17. Flowchart for the 6DOF POSE estimation during a dynamics simulation loop

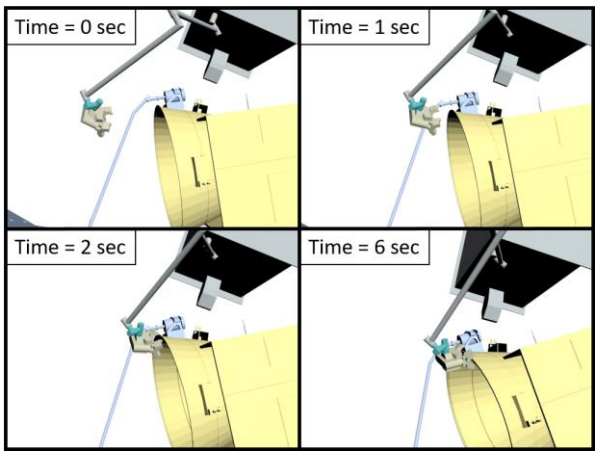

Fig. 18. LAR capture simulation with visual servoing

4.4 Compliant control simulations

A cartesian force/torque compliant control of the robotic arm will be used during the clamping operation. The goal of the compliant control is to ensure that during the motion of the arm the forces and torques (especially acting on the gripper) will be kept within a certain limit and that the gripper, the robotic arm and the clamp will not be damaged. In this case, it is necessary to control not only the position of the end-effector, but also the forces that arise when the manipulator interacts with the environment.

One of the approaches used to solve this problem is the impedance control approach [18] which is a type of the compliant control. The target impedance is defined as a mass-spring-damper system that is described by the following equation:

$$M_d(\ddot{X} - \ddot{X}_d) + B_d(\dot{X} - \dot{X}_d) + K_d(X - X_d) = -F_{ext} \quad (1)$$

where: M_d is the desired inertia matrix, B_d is the desired damping matrix, K_d is the desired stiffness matrix, X_d is a vector that represents the desired end-effector position, X is a vector that represents the actual end-effector position, F_{ext} are the external forces due to the interaction with the environment. Eq. (1) is used to define the trajectory which ensures that the target impedance is achieved.

Numerical simulations were performed to verify the proposed compliant control. These simulations were carried out using the 'Simulation tool for space robotics', which is being developed at CBK since 2009. The tool is based on the SimMechanics model of chaser satellite equipped with a 7 DOF robotic arm (SimMechanics is software based on the Simscape, the platform product for the MATLAB Simulink). The SimMechanics model of chaser is presented in Fig. 19. For the purpose of compliant control simulations in the frame of the e.Deorbit mission the simulation tool was updated. First, the model of Envisat was attached to the gripper and the robotic arm was changed to the specific arm proposed for this mission. The second modification is related to the robotic arm elasticity. In space elasticity is an important issue due to the lightweight structure of the arm. Preliminary simulations (based on mathematical models [10,20]) showed that for the e.Deorbit robotic arm the influence of elasticity in manipulator joints on the motion of the end-effector is much higher than the influence of elasticity of manipulator links. Therefore, in the compliant control simulations only the elasticity of manipulator joints is considered. The block representing the flexible joint is shown in Fig. 20. Such block was added in each joint of the robotic arm model. Another new feature, added to the simulation tool, is the model of contact. The contact between the clamp and LAR, occurring during the clamping operation, has significant influence on the behaviour of the system and must be taken into account.

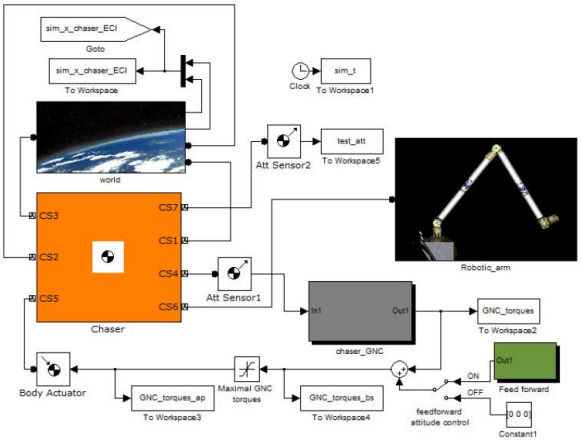

Fig. 19. SimMechanics model of the chaser satellite.

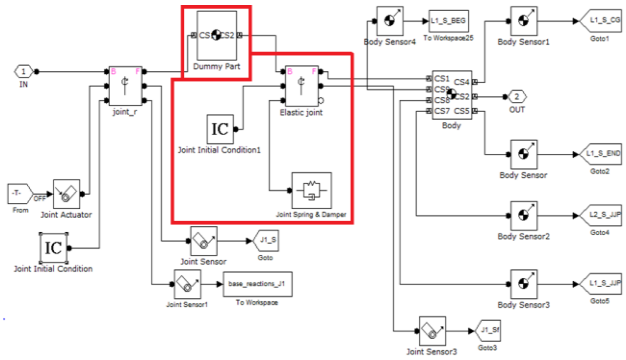

Fig. 20. SimMechanics model of flexible joint.

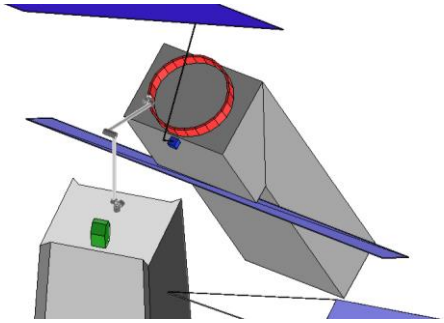

Fig. 21. Frame from animation showing chaser and Envisat before the clamping operation.

Validation of the proposed compliant control was performed using the Monte Carlo method. There were three main objectives of performed simulations: (i) to test the proposed compliant control for a wide range of parameters and initial conditions, (ii) to estimate forces and torques induced by the motion of the robotic arm when the gripper is attached to LAR, and (iii) to identify parameters that have the most significant influence on the overall performance of the compliant control. Initial assessment of obtained results shows that the proposed control is well suited for the clamping operation performed in the e.Deorbit mission. A frame from animation generated by the post-processing module of the simulation tool is presented in Fig. 21. This frame shows chaser and Envisat in the post-capture phase before the clamping operation.

5. Space tug definition

Considering the mission scenario, the e.Deorbit Spacetug has been customised from the Airbus Spacetug firstly dedicated to servicing in GEO. The reuse of such a generic vehicle addressing many in-orbit applications allowed maximising commonalities while minimizing adaptations and mission specific elements.

The general configuration of the e.Deorbit Spacetug is the following:

- A customized accommodation of the overall structure regarding RDV sensors, thruster architecture, antenna accommodation and capture system in accordance with the mission specificities.
- A full chemical propulsion system
  - 1x 430N Main Engine, mainly for deorbiting maneuvers
  - 22x 22N thrusters for Attitude Control and phasing with the target
  - 2x 22N thruster for detumbling along +Z-axis
  - 2 propellant tanks
  - 2 pressurant tanks
- An electrical power system based on a one wing rotating solar array (with two panels) and battery dimensioned for the mission
- GNC/visual navigation sensors mounted on the top floor:
  - Two LIDARs
  - Two wide angle cameras
  - Two narrow angle cameras
- Robotic arm on the +X side of the structure
- Clamping mechanism (accommodated on top panel) for attachment of the chaser on top of Envisat
- S-Band communication subsystems
- All platform electronic units are located on the +/-Y panels in order to optimize thermal control thanks to relevant heatpipe network

For AOCS purpose during absolute navigation phases and relative navigation (from rendezvous up until target fixation), a generic set of instruments is reused from Airbus Spacetug, as Star Trackers, sun sensors, etc. Additionally, GPS sensors have also been integrated to ease navigation.

In terms of functional architecture, the data handling subsystem (DHS) consists mainly of the on-board computer (OBC). The whole DHS will perform management of all platform and payload units. The OBC, reused from Airbus Spacetug design, allows control and data manages all the units. It is the central unit of the platform, acting as single master of all data buses. It implements classical functions from an OBC mainly for AOCS equipments and power management, and different modular boards dedicated to command/supply thermal lines or propulsion elements.

As the e.Deorbit Spacetug is a single mission vehicle, the electrical propulsion has been removed, therefore downsizing the overall electrical power system compared to the Airbus Spacetug dedicated to multi-mission services. Additionally, to comply with the duration of the mission, the overall Power subsystem has been downsized. It mainly consists on reducing the Solar Arrays configuration, adapting the Solar Arrays Drive Mechanism wrt this configuration, and a downscaled the battery. Here, Solar Array is derived from deployable SA Telecom Satellite as main e.Deorbit Spacetug structure is derived from standard Telecom Satellite line, allowing same use of HRMs (8

points). However, it will be limited to only a 2 panels configuration to fulfil power need.

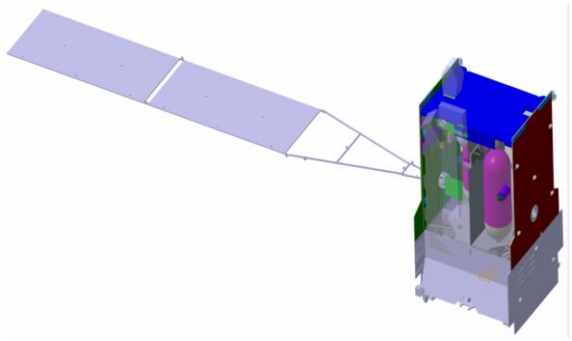

Fig. 22. Space Tug configuration.

In regards to mass budget and launcher, up to Phase B1 of the e.Deorbit mission, the European VEGA-C launch vehicle was planned to be used to inject the e.Deorbit chaser on the correct orbit to perform the mission. The VEGA-C payload capability with regard to the considered altitude and inclination ranges from 1500 to 1750kg approximately.

Due to e.Deorbit platform change (use of an Airbus Spacetug based vehicle), VEGA-C is no more foreseen, and even possible, considering the wet spacecraft mass and the overall dimensions of the complete vehicle.

As e.Deorbit Spacetug is based on Airbus Spacetug for servicing in GEO, it aims at being launched by a medium or heavy launcher. For example, from the Ariane 6 user manual, Ariane 62 launch capability in SSO (800km altitude with 98.6° of inclination) is above 5500kg. This initial performance provides a substantial mass margin with regard to the wet mass budget defined the e.Deorbit Spacetug vehicle.

In the current configuration, the e.Deorbit Spacetug wet mass is inferior to 3 tons, with a total propellant mass of about 950kg.

The initial assessment of the commonalities and differences between the Airbus Space Tug and a Space Tug based Chaser for e.Deorbit shows that a very high potential of synergies exists on the payload side for the robotic subsystem and the GNC including the visual-based navigation and tracking. This concerns also domains like the payload avionics and the FDIR. The verification and validation infrastructure for the payload could be shared between the two configurations. The operations can rely on the same concept, but maybe with different implementations, depending on the ESA and industrial strategies for the mission control center.

6. Robotic subsystem

The robotic subsystem will be used to capture, clamp, and assist in de-tumbling the target via the Launch Adapter Ring (LAR). It consists of following major elements.

- Robotic Manipulator (Arm): Used to manipulate the end effector to the capture point (LAR).
- LAR Gripper: The end effector of the robotic arm, used for capturing the Envisat's LAR.
- LAR Clamping Mechanism: This 2DOF clamp will rigidly secure Envisat to SpaceTug for deorbiting.
- Vision System: Used to navigate the LAR Gripper and Clamp towards the LAR using Visual Servoing. The vision system suite consists of three cameras and four laser pattern projectors.

An overview of the robotic payload system is depicted below in Fig. 23.

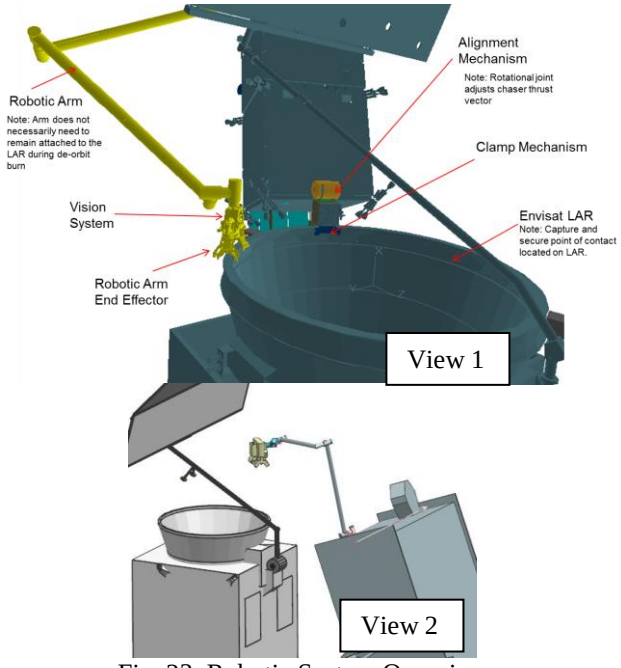

Fig. 23. Robotic System Overview

6.1 The Robotic Arm

The robotic arm is the primary physical interface between the Envisat and SpaceTug. It will be used to manuever the gripper to the capture point on the LAR, dampen residual motion between Envisat and the SpaceTug once captured, perform the clamping manoeuvre, and finally stabilize the solar array boom to assist with deorbiting. TABLE T2 provides a summary of key robotic arm values.

The arm will be mounted to SpaceTug, and consists of 7 joints to provide 7 Degrees of Freedom in a *'Roll, Yaw, Pitch, Pitch, Pitch, Yaw, Roll'* topology, providing the manipulability required by the e.Deorbit mission partial single-fault tolerance.

Table 1. Summary of Key Robotic Arm Values

Degrees Of Freedom	7
Length [m]	4.39
Output Torque [Nm]	200
Peak Output Torque [Nm]	314
Mass [kg]	52.43 (59.92 w/ Margin)
Stowed Volume [cm]	226.5 X 123.9 X 24

Fig. 24. shows the layout of the Robotic Arm.

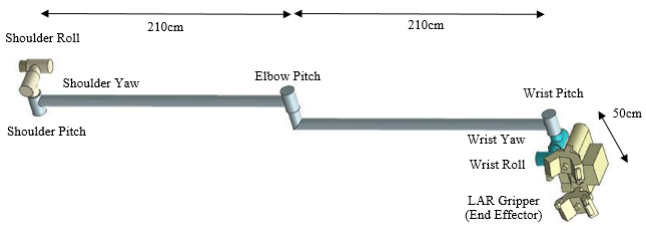

Fig. 24. Robotic Arm Layout

6.2 The LAR Gripper

The LAR Gripper will be used to capture the Envisat's LAR. It is guided into position using the robotic manipulator and visual servoing. Once aligned, the gripper initiates capture consisting of a fast "soft capture" followed by a slower rigidizing for "hard capture". Once the "hard capture" is complete, the LAR is fully secured by the gripper. An illustration of the final LAR Gripper designed for e.Deorbit is provided in Fig. 25.

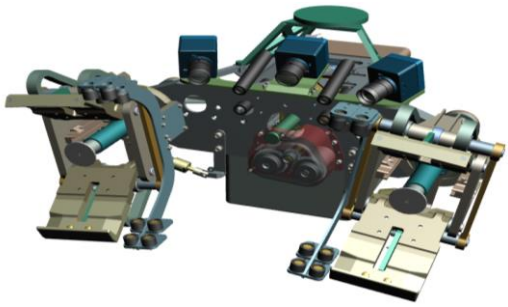

Volume: 575mm x 524mm x 310mm
Fig. 25. LAR Gripper

This LAR Gripper incorporates the following main subsystems and hardware:

- A **Grasping Mechanism** to achieve connection to the LAR. The grasping mechanism is comprised of jaw assemblies, trigger mechanisms, a drive assembly, and controller electronics.
- A **Vision System** which is comprised of two sub-systems;
  - A Situational Awareness Subsystem to support the visual monitoring of the capture operation.
  - A Pose Estimation Subsystem, consisting of laser pattern projectors, monochrome cameras, and optical filters, to enable the determination of the pose of the Envisat LAR.
- A **Thermal Control** subsystem.

7. Clamping subsystem

Clamping mechanism's (CLM) role is to provide a rigid connection between ENVISAT's Launch Adapter Ring (LAR) and Space Tug during e.Deorbit mission's clamping and disposal phases.

Clamping mechanism is mounted on the top panel of Space Tug spacecraft.

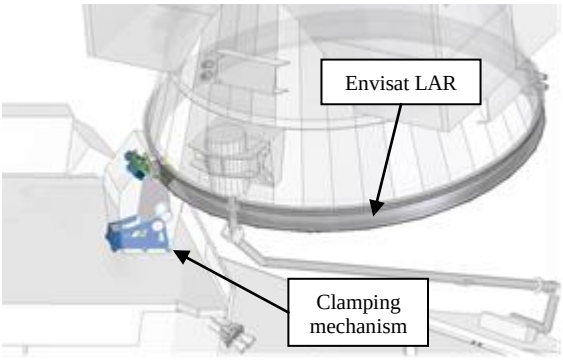

Fig. 26. Location of the clamping mechanism on the Space Tug's top panel.

CLM's development started during Phase B1 of e.Deorbit mission. The current design combines the most promising solutions considered in trade-offs. It can be divided into two sub-mechanisms (Fig. 27):

- Fixing mechanism – consists of clamps, (fixed and rotary), sensors (visual, proximity, force, light curtains) and linear actuator used for clamps operations
- Alignment mechanism – linear actuator and linkage allowing for adequate modification of clamping mechanism's angular position in order to set Space Tug's thrust vector in line with ENVISAT's CoG (trimming).

Clamping mechanism is actuated when presence of the LAR between the clamping mechanism's jaws is confirmed by information received from sensors. It is based on lead screw assembly and linkage mechanism that rotates and the rotary clamp and keeps it in its 'clamped' position. In addition, rolling elements are used to assure the optimal contact (shape and friction),

preload, thermal isolation and mitigate risk of cold welding (Fig. 28).
The expected motion range and resolution in case of the proposed design are the following:

- Angular range of the clamps: approx. 0-30°
- Resolution: approx. 0,01° rotary, 250 µm linear (not a critical design driver – rotary clamp's main task is to achieve the maximum possible position and apply preload on the LAR).

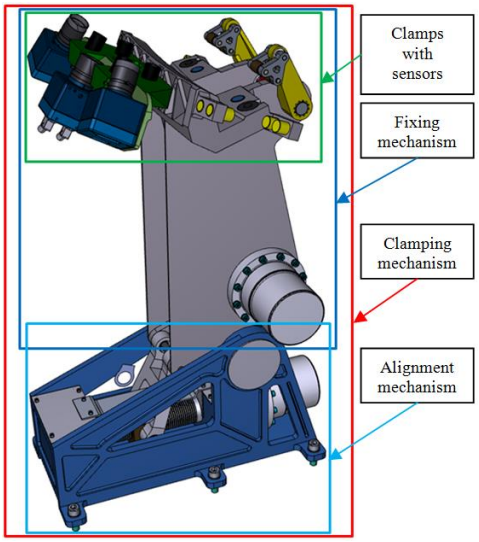

Fig. 27. Clamping mechanism

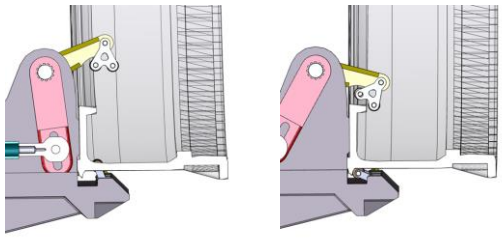

Fig. 28. Clamping mechanism's operation

The main considerations are as follows:

- Condition of the interfaces on ENVISAT (e.g. silvered Teflon® tape on the LAR, CFRP and MLI degradation due to e.g. atomic oxygen, UV radiation or meteoroid impacts)
- Rigidity of the clamping mechanism's structure. High stiffness of the connection between ENVISAT and Space Tug is foreseen in order to transfer the loads during disposal phase and avoid certain stack natural frequencies, e.g. frequency close to sloshing.
- Ability to adapt to encountered obstacles and shapes (rollers) during clamping operation and to preload the connection.

Further development of the clamping mechanism has to be adapted and optimised to cope with the mentioned above considerations.

8. Innovative solutions

In the course of the e.Deorbit studies, innovative solutions were identified in the following domains:

- In-orbit characterization of the Target based on measurements from Chaser sensors
- Navigation to uncooperative Targets in all lighting conditions
- Contactless detumbling operations of the Target
- Synchronized flight with the Target
- Capture and stabilization of a tumbling Target with a robot arm in compliant mode
- Gripper integrating fast soft capture and grasp rigidization, and light-independent sensor system for visual tracking
- Coupled-control between the Chaser platform and the robotics
- Full automatic robotic system with optional ground supervision
- Onboard monitoring concept for safe automatic operations
- Definition of a robust communications concept including onboard communications architecture and ground station selection
- Concept of operations with onboard and on-ground activity sharing
- Reuse of the GEO-Servicing Airbus Space Tug for other on-orbit servicing missions like debris removal
- Implementation of a MBSE process based on SysML and vehicle database

These innovative solutions could be first fully validated in the e.Deorbit mission, and then further deployed in on-orbit servicing missions like the GEO Servicing and exploration missions.

9. Conclusion

Central to the e.Deorbit mission is the rendezvous of a Space Tug with a defunct satellite followed by its capture, stabilisation, fixation and disposal. An important part of the Space Tug properties are related to safety for avoiding the generation of new debris due to potential collisions and also to mission efficiency.

Over the e.Deorbit studies [21, 22] completed by this Consolidation Phase major achievements were made on the definition of the mission phases and activities, the architectures and their dependencies, the system limitations w.r.t. the Target tumbling rate, the required system performances, the safety approach, the communication blockage aspects, the autonomy concept and operations, the reuse approach for other OOS missions [23] and in general on the system definition to implement a safe active debris removal.

The new selected ENVISAT tumbling rate of 2,5deg/s can be reduced to 0,5deg/s thanks to the contactless detumbling of the ENVISAT using specific Space Tug thrusters. This relaxes requirements on the propulsion and robot arm subsystem which where otherwise at the limit of their performance. Overall the system safety can be increased with this updated Target behaviour.

New technologies with an actual TRL below 6, such as the visual based navigation (camera and image processing), robot joint, gripper, clamping mechanisms, monitoring software and payload computer, will also need further technology development, as planned by ESA in the coming e.Deorbit technology maturation phase.

Additionally, during the Airbus DS-led study it was shown that the architectures and technologies selected for the system comply with the required industrial point cost estimate of 150M€ for the phases B2/C/D/E1.

Acknowledgements

This work was performed under ESA contract (e.Deorbit Consolidation Phase), funded by ESA's General Support Technology Programme.

References

[1] ESA's Space Debris Office (BR-309 March 2013), September 2012

[2] The IADC is an international forum of space agencies for the worldwide coordination of activities related to the issues of man-made and natural debris in space (www.iadc-online.org)

[3] Space Debris Mitigation Guidelines of the United Nations Committee on the Peaceful Uses of Outer Space (UN COPUOS, 2007); these guidelines are largely based on the IAADC Space Debris Mitigation Guidelines.

[4] Space Debris, IADC Assessment Report for 2011 (IADC-12-06, April 2013)

[5] Stability of the Future LEO Environment (IADC-12-08, Rev. 1, January 2013)

[6] IADC Presentation to 50th UNCOPUOS STSC (IADC-13-01, February 2013)

[7] T.V. Peters, D. Escorial Olmos, Applicability of COBRA concept to detumbling space debris objects, Proceedings of the 6th international conference on astrodynamics tools and techniques, 2016.

[8] S. Vanden Bussche, A. Lakusiak, C. Imhof, K. Symonds, R. Biesbroek, D. Gerrits, S. Estable, Supervising the capture of a large, tumbling satellite: Communication challenges, TTC, ESTEC, 13 – 16 September 2016

[9] F. Ankersen, Guidance, Navigation, Control and Relative Dynamics for Spacecraft Proximity Manoeuvres, PhD Thesis, 2010.

[10] T.V. Peters, N.M.G. Paulino, F. Gandía, Investigation of Active Detumbling Solutions for Debris Removal, Clean Space Industrial Days, ESA/ESTEC, Netherlands, 2016, 23-27 May.

[11] D. Alazard, J.-A. Perez-Gonzalez, T. Loquen, C. Cumer, Two-input two-output port model for mechanical systems, Scitech 2015 - 53rd AIAA Aerospace Sciences Meeting, Kissimmee, United States, 2015, 15 January

[12] D.E. Olmos, T.V. Peters, J. Naudet, C.C. Chitu, K. Sewerin, ANDROID Small Active Debris Removal Mission, 5th CEAS Air and Space conference, Delft, Netherlands, 2015, 7 – 11 September.

[13] F. Ankersen, A Mathematical Approach to Monte Carlo Simulations and their Statistical Post Processing, EWP 2271, ESA, 2002.

[14] Doyle, J.C., K. Glover, P.P. Khargonekar, B.A. Francis, State-space solutions to standards H2 and Hinf control problems, IEEE Transactions on Automatic Control, vol. AC-34, no. 8, pp. 831-847, 1989.

[15] Doyle, J.C., Robust and optimal control, Proceedings of the 35th Conference on Decision and Control, Kobe, Japan, Conference Proceedings, pp. 1595 – 1598, 1996.

[16] J.F. Vasconcelos et al., GNC design and validation for rendezvous, detumbling, and de-orbiting of ENVISAT using a clamping mechanism, 6th International Conference on Astrodynamics Tools and Techniques, Darmstadt, Germany, March 2016.

[17] Telaar, J., Estable, S., et al. 2017. Coupled Control of Chaser Platform and Robot Arm for the e.Deorbit Mission, 10th International ESA Conference on Guidance, Navigation & Control Systems, Salzburg, Austria

[18] N. Hogan, Impedance Control: An approach to manipulation: I-Theory, II-Implementation, III-Applications, ASME Transactions Journal of Dynamic Systems and Measurement Control B 107 (1985) 1-24.

[19] A. Green, J.Z. Sasiadek, Adaptive Control of a Flexible Robot Using Fuzzy Logic, Journal of Guidance, Control, and Dynamics 28(1) (2005) 46-42.

[20] S. Ulrich, J.Z. Sasiadek, I. Barkana, Modeling and Direct Adaptive Control of a flexible-Joint Manipulator, Journal of Guidance, Control, and Dynamics 35(1) (2012) 25-39.

[21] Airbus DS (2014). Edeorbit Final Report Phase A. EDEORBIT-ASD-RP-0009-1.0_Final_Report. ESA

[22] Airbus DS (2016). Edeorbit Final Report Phase B1. EDEB1-RIBRE-RP-0020-1.0_Final_Report. ESA.

[23] Pisseloup, Aurélien et al. (2016). Airbus Defence and Space's vision and activities in active debris

removal and on-orbit servicing. 67th International Astronautical Congress.